Iranian Journal of Astronomy and Astrophysics
Vol. 12, No. 2, Spring 2025, 143–161
©Available online at http://ijaa.du.ac.ir
DOI: 10.22128/ijaa.2025.2992.1216
Online ISSN: 2383–403X

Iranian Journal of Astronomy and Astrophysics

Research Paper

Numerical Study of Magnetoacoustic Wave Interaction with Null Points: Plasma Beta Modulation in Solar Atmospheres

Naser Karimi*[1] · Mahdi Alizadeh[2] · Zianab Shajei[3] · Ehsan Tavabi[5] · Navid Elyasi[5]

[1] Department of Physics Education, P.O. Box 14665–889, Frahangian University, Tehran, Iran;
*E-mail: n.karimi@cfu.ac.ir

[2] Independant researcher, Tabriz, Iran;
E-mail: mah.alizadeh1997@gmail.com

[3] Physics Department, Payame Noor University, Tehran, 19395–3697, Iran;
E-mail: zshaji1107@gmail.com

[4] Physics Department, Payame Noor University, Tehran, 19395–3697, Iran;
E-mail: e_tavabi@pnu.ac.ir

[5] Department of Electrical Engineering, Chalmers University of Technology, Gothenburg, Sweden;
E-mail: navid.elyasi97@gmail.com

Received: 15 July 2025; **Accepted:** 27 Septembere 2025; **Published:** 8 October 2025

Abstract. This investigation examines the interaction of magnetoacoustic pulses with a two-dimensional magnetic null point, explicitly accounting for variations in plasma β arising from spatial fluctuations in the magnetic field strength. The analysis employs the PLUTO code to solve the magnetohydrodynamic (MHD) equations, enabling a detailed exploration of nonlinear effects associated with plasma β modulation across distinct stratified layers. The results demonstrate temporal evolution in the system's response, characterized by periodic fluctuations in amplitude and the emergence of pronounced peaks. These features indicate episodes of intensified coupling between the magnetoacoustic pulses and the magnetic topology. The observed variability in both amplitude and peak sharpness underscores the system's inherent dynamism, with certain temporal phases exhibiting more vigorous interactions. Furthermore, the study reveals a correlation between plasma density alterations and radial velocity variations of the pulses, suggesting that these phenomena are closely tied to the redistribution of plasma β throughout the stratified magnetic environment.

Keywords: Sun, Magnetohydrodynamics, Magnetoacoustic Wave Dynamics, 2D Magnetic Null Point, Plasma Beta.

1 Introduction

The phenomenon of coronal heating represents a pivotal and intricate component of solar atmospheric dynamics. Elucidating the mechanisms responsible for plasma heating in the solar corona remains a formidable scientific challenge [1]. Two primary theoretical frameworks, wave-based heating and magnetic reconnection, offer distinct explanations for the elevated temperatures of the solar corona, substantiated by empirical evidence of oscillatory phenomena and magnetic reconnection events observed in solar observations.

* *Corresponding author*

Magnetic reconnection is an event that occurs when the structure of the plasma magnetic field undergoes changes [2–4]. A reconnection site is associated with a magnetic null point, defined as a location within a reconnection region where the magnetic field strength is zero. These regions, characterized by the absence of magnetic field intensity, significantly affect wave propagation due to the intricate balance between magnetic forces and plasma pressure.

Magnetic reconnection is a well-established mechanism for initiating various solar phenomena, playing a pivotal role in the dynamic processes central to coronal seismology. This mechanism is fundamental in plasma physics, as it facilitates the rapid release of energy stored within magnetic field configurations, converting it into thermal and kinetic energy. This energy transformation results in plasma heating, large-scale plasma flows, and particle acceleration.

In the solar corona, magnetohydrodynamic (MHD) waves and magnetic reconnection are frequently analyzed independently, despite their strong interdependence. Notably, intense magnetic reconnection events can generate waves that perturb magnetic null points, potentially triggering subsequent reconnection processes [5–7]. The transient behavior of linear waves near null points, along with its implications for solar physics, has been extensively studied [8]. A direct observation of a fast wave interaction with a coronal null point is presented in Ref. [9].

Magnetoacoustic waves play a fundamental role in the dynamics of astrophysical plasmas, particularly in the solar corona and the Earth's magnetosphere, where complex magnetic topologies such as null points are prevalent. The interaction of magnetoacoustic waves with null points in plasma is a fundamental aspect of plasma physics that holds significant implications for various astrophysical and laboratory contexts [10].

A numerical experimental setup that considers solar coronal conditions is employed to investigate the effect of magnetoacoustic waves on the generation of plasmoid ejections [11]. Central to this interaction is the plasma beta (β) parameter, which quantifies the ratio of thermal pressure to magnetic pressure within the plasma. Understanding how magnetoacoustic waves behave in relation to this parameter is crucial for elucidating wave dynamics, particularly in environments such as the solar atmosphere and laboratory fusion plasmas [5,12].

As the magnetic field topology varies spatially, plasma β naturally fluctuates, profoundly affecting wave dynamics and nonlinear effects [13]. In the solar corona, for instance, plasma β is typically much less than one, allowing for the simplification of governing equations by neglecting pressure gradients. However, this parameter is not uniform; it fluctuates across different regions due to the complex interplay of magnetic fields [8]. Near magnetic null points, where the magnetic field strength diminishes, plasma β can increase significantly, altering the characteristics of wave interactions.

This research examines the dynamics of magnetoacoustic pulses interacting with a two-dimensional magnetic null point, with an emphasis on nonlinear effects driven by variations in the plasma beta parameter. The study specifically investigates how plasma β influences different atmospheric layers by analyzing changes in plasma density and radial velocity profiles.

Numerical simulations were performed using the PLUTO code [14,15], a finite-volume, shock-capturing computational framework that employs double-precision arithmetic for enhanced accuracy. The subsequent section details the governing equations and initial conditions [16]. Section 3 describes the simulation of the magnetoacoustic wave's interaction with the magnetic null point. Results and their implications are discussed in Section 4, while Section 5 provides a succinct summary and prospects for future investigations.

2 Model and Analytical Framework

Within the scope of this investigation, our computational findings are grounded in magnetohydrodynamic (MHD) theory, extending the foundational work of Gruszecki et al. [17].

The developed model accounts for finite plasma-β conditions. It is pertinent to emphasize the standard resistive MHD equations, formulated in the absence of gravitational effects, which are presented below

$$\frac{\partial \rho}{\partial \mathrm{t}} + \nabla . (\rho \mathbf{v}) = 0, \tag{1}$$

$$\rho \left[\frac{\partial \mathbf{v}}{\partial \mathrm{t}} + \rho (\mathbf{v} . \nabla) \mathbf{v} \right] = -\nabla \mathrm{P} + \frac{1}{\mu} (\nabla \times \mathbf{B}) \times \mathbf{B}, \tag{2}$$

$$\rho \left[\frac{\partial \epsilon}{\partial \mathrm{t}} + (\mathbf{v} . \nabla) \epsilon \right] = -\mathrm{P} \nabla . \mathbf{v} + \frac{1}{\sigma} |\mathbf{J}|^2 + \Lambda, \tag{3}$$

$$\frac{\partial \mathbf{B}}{\partial \mathrm{t}} = \nabla \times (\mathbf{v} \times \mathbf{B}) + \eta \nabla^2 \mathbf{B}. \tag{4}$$

It is essential to underscore that the magnetic field $\mathbf{B}$ satisfies the divergence-free condition, $\nabla .\ \mathbf{B} = 0$, and the electric current density $\mathbf{J}$ is defined as $\mathbf{J} = (\nabla \times \mathbf{B})/\mu$. The physical parameters ρ, p, and $\mathbf{v}$ represent the plasma density, pressure, and velocity vector, respectively. In this context, $\mu = 4\pi \times 10^{-7}\ Hm^{-1}$ denotes the magnetic permeability, while σ represents the electrical conductivity, inversely related to the magnetic diffusivity η. The internal energy density ϵ is given by $\epsilon = \mathrm{p}/[\rho(\gamma - 1)]$, where γ, the adiabatic index, is assigned a value of 5/3.

The analysis focuses on a stationary, uniform medium characterized by constant density and pressure (ρ_0, p_0), embedded within an initial equilibrium magnetic field. The methodology employs linearization of the MHD equations, assuming small perturbations. Starting from the fundamental MHD equations, which describe the behavior of a fully ionized plasma approximated as an ideal gas, the continuity equation is applied. With $\Lambda = \eta = 0$, and using subscripts 0 and 1 to denote equilibrium and perturbed quantities, respectively, the linearized equation of motion is formulated as follows

$$\frac{\partial \rho_1}{\partial t} + \rho_0 \boldsymbol{\nabla} . \boldsymbol{v_1} = 0, \tag{5}$$

$$\rho_0 \frac{\partial \boldsymbol{v_1}}{\partial t} + \boldsymbol{\nabla} p_1 = (\ \boldsymbol{\nabla} \times \boldsymbol{B_1}) \times \boldsymbol{B_0}, \tag{6}$$

$$\frac{\partial \boldsymbol{B_1}}{\partial t} - \boldsymbol{\nabla} \times (\boldsymbol{v_1} \times \boldsymbol{B_0}) = 0, \tag{7}$$

$$\frac{\partial p_1}{\partial t} + \gamma p_0 \boldsymbol{\nabla} . \boldsymbol{v_1} = 0, \tag{8}$$

$$(\ \boldsymbol{\nabla} . \boldsymbol{B_1}) = 0. \tag{9}$$

The initial equilibrium magnetic field [18, 19], is described as $\mathbf{B} = \mathbf{B}_0[\mathrm{x/L}, -\mathrm{y/L}, 0]$, where B_0 represents the magnetic field strength and L denotes a characteristic length scale. This refers to a state in which the forces acting on the plasma ions and charged particles are in equilibrium. This state is essential for understanding how magnetic fields influence fluid motions and wave propagation within a plasma. In astrophysical contexts, such as solar physics or space weather, equilibrium configurations often describe the structure of coronal magnetic fields, where the magnetic field is typically force-free, with magnetic tension dominating over plasma pressure and gravity, though gradients in magnetic pressure contribute

to the force balance near null points. Throughout much of the corona, the plasma β is considerably less than one, allowing us to disregard pressure gradients in the plasma. However, near null points, the magnetic field diminishes, leading to a potential rise in plasma β.

$$\beta = \frac{2\mu \mathrm{p_0}}{\mathrm{B}^2} \quad \Longrightarrow \quad \beta = \frac{\beta_0}{\mathrm{x}^2+y^2} = \frac{\beta_0}{\mathrm{r}^2}, \tag{10}$$

where

$$\mathrm{r}^2 = \mathrm{x}^2+\mathrm{y}^2 \qquad \beta_0 = \frac{2\mu \mathrm{p_0 L}^2}{\mathrm{B}_0^2}. \tag{11}$$

The plasma β parameter exhibits spatial variation across the modeled domain, driven by the dynamic evolution of the magnetic field. In regions devoid of a guiding magnetic field, plasma β approaches infinity at the null point, where the magnetic field strength diminishes to zero. Specifically, beyond a radial distance of unity, a low-β regime dominates, whereas a high-β environment is observed within this radius. This variation significantly influences the behavior of fast and slow magnetoacoustic waves, which manifest distinct characteristics contingent upon the local plasma conditions. To investigate the dynamics of magnetoacoustic waves in proximity to a two-dimensional magnetic null point, the system is initialized by introducing a perturbation from its equilibrium state. This is achieved by generating a circular fast magnetoacoustic pulse, centered at the origin, with a circumference defined as $2\pi r_1$, as described by the governing equations outlined below [5].

$$V_\perp(x,y) = A_0 \sin\left(\pi \frac{\sqrt{x^2+y^2} - r_1}{r_0}\right),$$

$$\mathrm{V}_\parallel = 0, \tag{12}$$

where

$$\begin{aligned} \mathrm{V}_\perp &= (\mathrm{V}\times\mathrm{B}).\hat{z} = \mathrm{v_x B_y - v_y B_x}, \\ \mathrm{V}_\parallel &= \mathrm{v_x B_x + v_y B_y}. \end{aligned} \tag{13}$$

In a Cartesian coordinate framework, the system is described as follows

$$\begin{aligned} \mathrm{v_x} &= \frac{\mathrm{V}_\parallel \mathrm{B_x} + \mathrm{V}_\perp \mathrm{B_y}}{|\mathrm{B}|^2}, \\ \mathrm{v_y} &= \frac{\mathrm{V}_\parallel \mathrm{B_y} - \mathrm{V}_\perp \mathrm{B_x}}{|\mathrm{B}|^2}. \end{aligned} \tag{14}$$

The velocity distribution of the initial magnetoacoustic pulse within the x-y plane is expressed as follows

$$\mathrm{v_x} = \mathrm{A_0 sin}\left(\pi \frac{\sqrt{\mathrm{x}^2+\mathrm{y}^2} - \mathrm{r_1}}{\mathrm{r_0}}\right) \frac{\mathrm{B_y}}{\mathrm{B_x}^2 + \mathrm{B_y}^2}, \tag{15}$$

$$\mathrm{v_y} = -\mathrm{A_0 sin}\left(\pi \frac{\sqrt{\mathrm{x}^2+\mathrm{y}^2} - \mathrm{r_1}}{\mathrm{r_0}}\right) \frac{\mathrm{B_x}}{\mathrm{B_x}^2 + \mathrm{B_y}^2}. \tag{16}$$

In the region surrounding a magnetic null point, the spatial domain is defined by the condition $r_1 < \sqrt{x^2+y^2} < r_1 + r_0$, where the velocity component $v_z = 0$, and the initial amplitude of the circular magnetoacoustic pulse is set to $A_0 = 1$.

3 Numerical Setup

Previous investigations into nonlinear waves in the solar atmosphere have particularly focused on coronal heating. The study of fully nonlinear problems is feasible only through numerical methods. In our experiments, an initially symmetric nonlinear fast magnetoacoustic pulse is initiated at a specific distance from a magnetic null point and directed toward the isothermal null point. In equations 6 and 7, the coefficient A_0 indicates whether the pulse is linear or nonlinear. The small A_0 (e.g., $A_0 << 1$) corresponds to linear behavior, while larger A_0 (e.g., $A_0 \approx 1$) indicates nonlinear behavior, though nonlinearity can emerge at amplitudes below unity depending on plasma conditions. Here, we consider a nonlinear pulse, specifically A_0=1. Note that although in Section 2 we referred to linear MHD equations to understand the fundamental wave dynamics, we do transition to numerical simulations that incorporate non-linear effects. This ensures that the study captures both linear and non-linear phenomena. In fact, the PLUTO code enables solving the full nonlinear MHD equations in one to three dimensions. This investigation extends the foundational research of Karampelas et al.[16], focusing on plasma density perturbations driven by variations in atmospheric parameters, particularly the plasma-β parameter.

The numerical simulations utilize the PLUTO code, a robust tool for magnetohydrodynamic (MHD) modeling, employing a finite-volume, shock-capturing methodology. In a Cartesian coordinate system, the temporal evolution is computed using a third-order Runge-Kutta method for time stepping. Spatial integration is performed with a fifth-order monotonicity-preserving scheme (MP5), coupled with the total variation diminishing Lax-Friedrich solver (TVDLF). To ensure adaptability to diverse solar atmospheric conditions and plasma-β regimes, the code variable U_c is normalized relative to U_0.

The computational domain encompasses a region of (-10, 10) × (-10, 10) Mm, discretized with a grid resolution of 2500 × 2500 points. Zero-gradient boundary conditions are applied to maintain numerical stability. The PLUTO code employs dimensionless quantities, necessitating the specification of three fundamental parameters: the reference density $\rho_0 = 10^{-12} kg/m^3$, the reference length $L_0 = 10^6 m$, and the reference magnetic field strength $B_0 = 10^{-3} T$. The reference velocity is defined as $v_0 = \frac{B_0}{\sqrt{\mu \rho_0}}$, ensuring a constant background Alfvén speed, where μ represents the magnetic permeability. Additionally, the radial parameters are set as $r_1 = 5$ Mm and $r_0 = 1$ Mm.

This study investigates the dynamics of nonlinear fast magnetoacoustic waves with an initial amplitude $A_0 = 1$, across radial layers defined at $r = 1$, r = $\frac{1}{\sqrt{10}}$, and r = $\frac{1}{10}$. The analysis focuses on perturbations in plasma density and radial velocity induced by the propagation of these waves, accounting for spatial variations in plasma β due to fluctuations in the magnetic field. To explore these phenomena, a symmetric fast magnetoacoustic wave is introduced, enabling the examination of nonlinear interactions with magnetic null points within the context of MHD wave dynamics and coronal heating processes.

4 Results and discussion

During the propagation of magnetohydrodynamic (MHD) waves, fluctuations in plasma density, pressure, and temperature are observed. Figures 1 through 4 depict the radial velocity profiles of a magnetoacoustic pulse as it approaches a magnetic null point under two distinct atmospheric conditions, characterized by plasma β values of approximately $\beta_0 \approx 0$ and $\beta_0 = 1$, across radial layers at r = 1, r = 0.32, and r = 0.1. These profiles are captured in seven temporal snapshots at t = 0 s, t = 0.4 s, t = 1 s, t = 2 s, t = 2.5 s, t = 3 s, and t = 4 s. Initially, the pulse bifurcates into two distinct waves due to spatial variations in

phase velocity: an outward-propagating wave and an inward-propagating wave. The analysis focuses on the inward wave directed toward the null point. The pulse's geometry transitions from a circular to an elliptical configuration, influenced by the azimuthal dependence of the nonlinear coefficient [17].

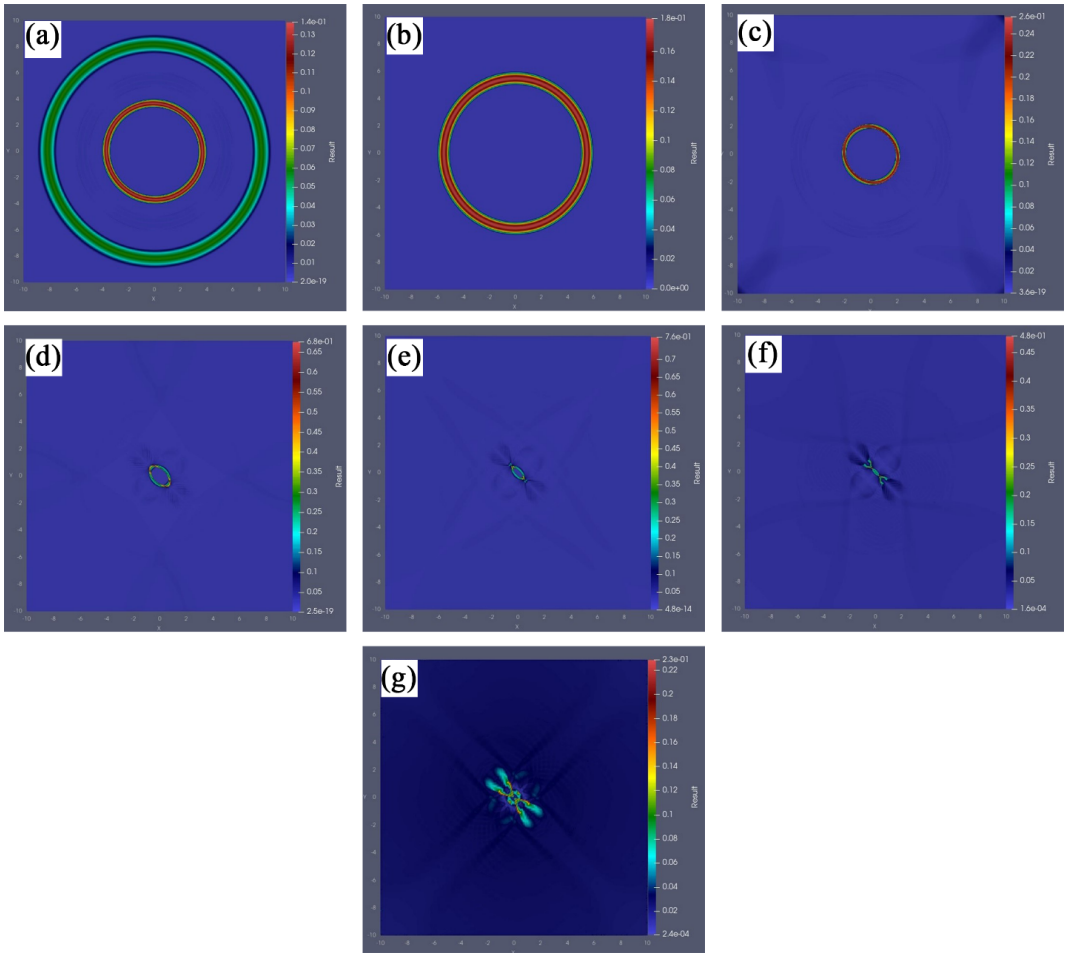

Figure 1: Temporal profiles of the radial velocity for the inward-propagating rarefaction pulse, defined as $v_r = \sqrt{v_x^2 + v_y^2}$, are presented as functions of the radial coordinate r for a plasma β value of approximately $\beta_0 \approx 0$, evaluated at radial positions r = 1, r = $\frac{1}{\sqrt{10}}$, and r = = $\frac{1}{10}$. These profiles are captured at the following time instances: a) t = 0 s, b) t = 0.4 s, c) t = 1 s, d) t = 2 s, e) t = 2.5 s, f) t = 3 s, and g) t = 4 s.

Figures 1 through 4 depict the variations in the radial velocity of the magnetoacoustic pulse as a function of the plasma β parameter and the radial distance of the layers from the magnetic null point. For enhanced clarity, Figure 9 presents the absolute values of the radial velocity along the diagonal line defined by y = x. The scaleless nature of the 2D null point model implies that the behavior shown in Figures 1–4 is qualitatively similar for waves initiated at different distances from the null point, relative to the $\beta = 1$ circle. However, the magnitude of nonlinear effects and pulse shape changes depends on the initial distance,

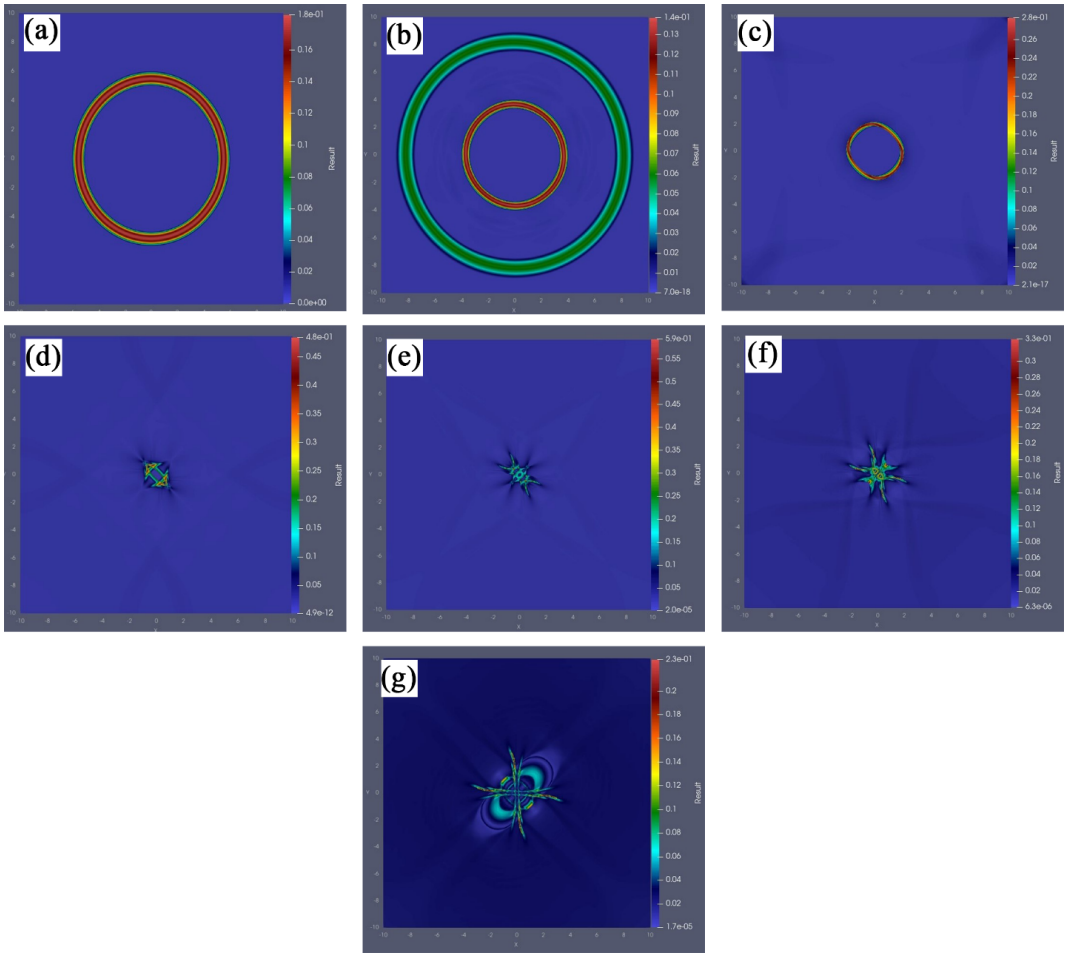

Figure 2: Temporal snapshots of the radial velocity for the inward-propagating rarefaction pulse, expressed as $v_r = \sqrt{v_x^2 + v_y^2}$, are presented as functions of the radial coordinate r, with a plasma β value of $\beta_0 = 1$, evaluated at the radial position r = 1. These profiles are captured at the following time points: a) t = 0 s, b) t = 0.4 s, c) t = 1 s, d) t = 2 s, e) t = 2.5 s, f) t = 3 s, and g) t = 4 s.

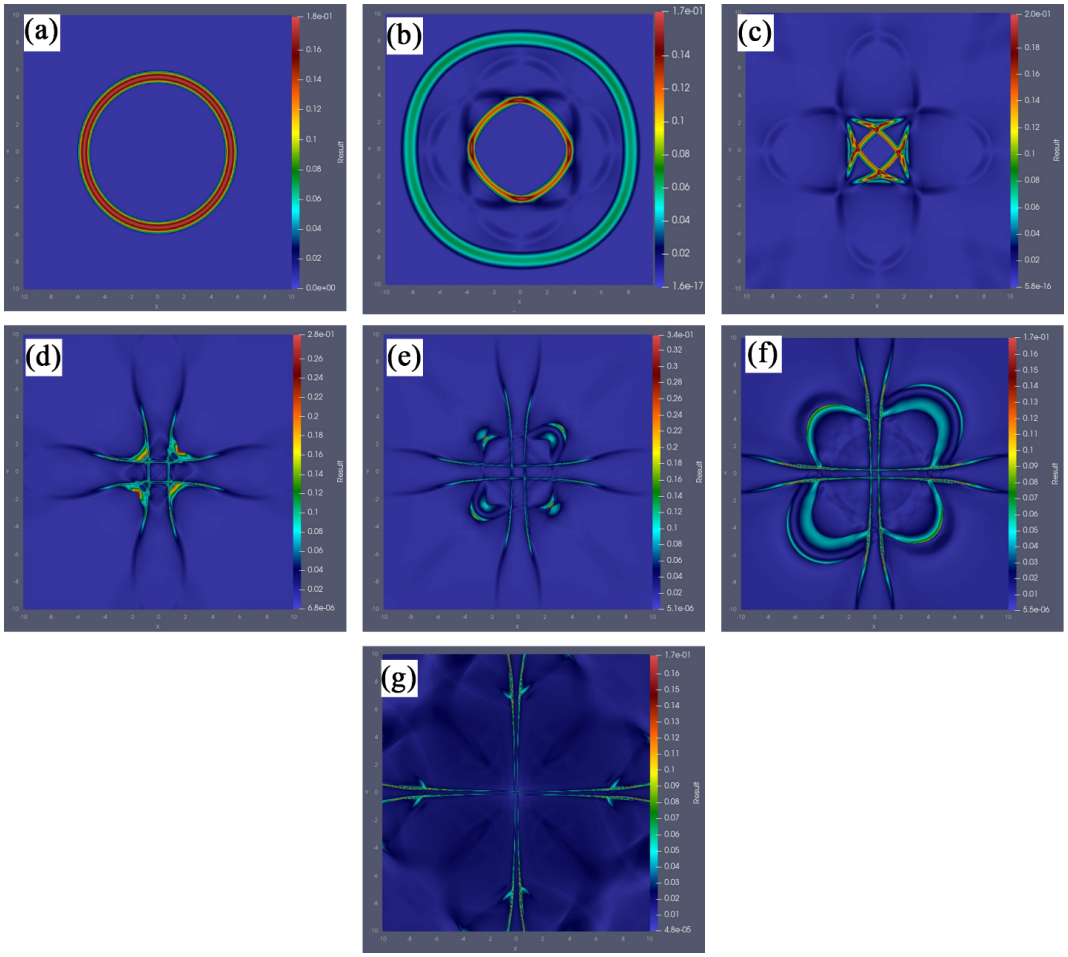

Figure 3: Temporal profiles of the radial velocity for the inward-propagating rarefaction pulse, defined as $v_r = \sqrt{v_x^2 + v_y^2}$, are presented as functions of the radial coordinate r, with a plasma β value of $\beta_0 = 1$, evaluated at the radial position $r = \frac{1}{\sqrt{10}}$. These profiles are captured at the following time instances: a) $t = 0$ s, b) $t = 0.4$ s, c) $t = 1$ s, d) $t = 2$ s, e) $t = 2.5$ s, f) $t = 3$ s, and g) $t = 4$ s.

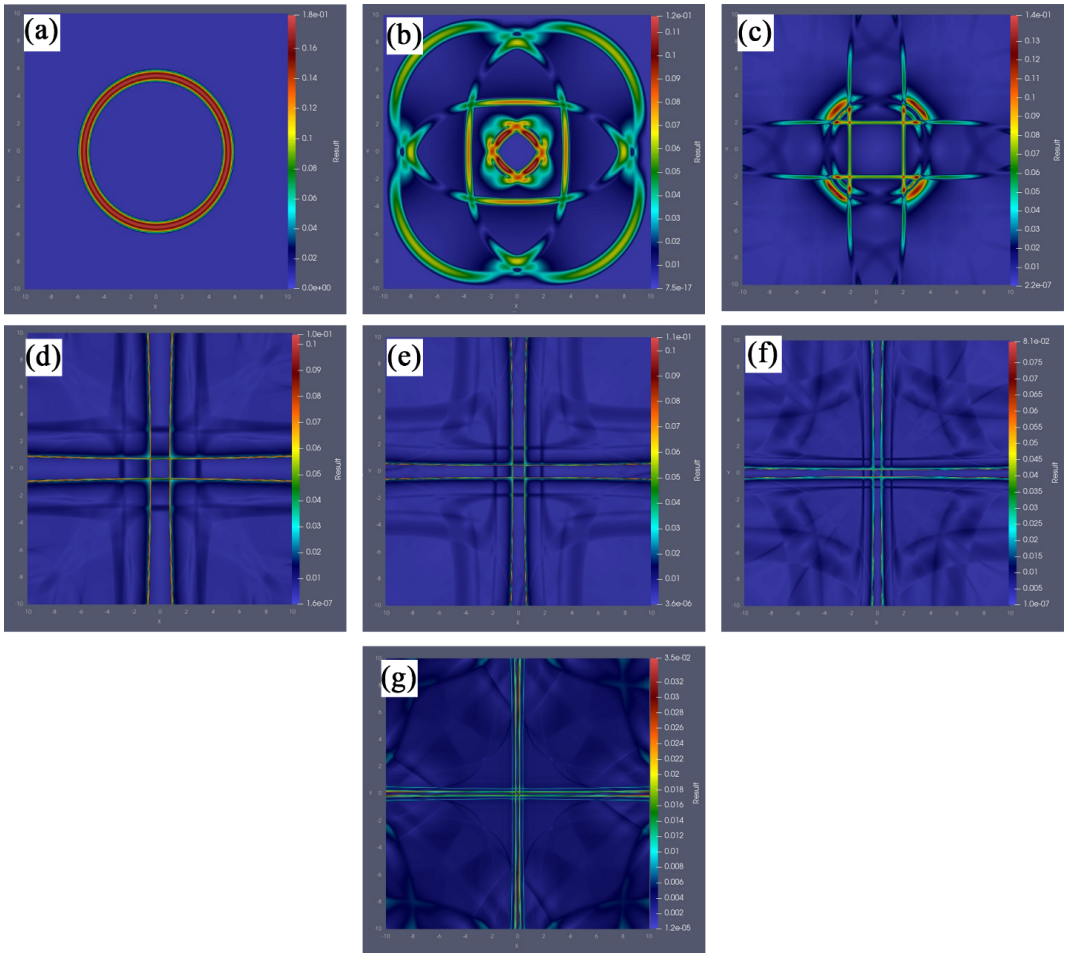

Figure 4: Temporal profiles of the radial velocity for the inward-propagating rarefaction pulse, expressed as $v_r = \sqrt{v_x^2 + v_y^2}$, are presented as functions of the radial coordinate r, with a plasma β value of $\beta_0 = 1$, evaluated at the radial position $r = 0.1$. These profiles are captured at the following time points: a) $t = 0$ s, b) $t = 0.4$ s, c) $t = 1$ s, d) $t = 2$ s, e) $t = 2.5$ s, f) $t = 3$ s, and g) $t = 4$ s.

with closer initiation (e.g., within r = 1) amplifying nonlinear interactions due to higher β values." This clarifies the model's flexibility and limitations.

To draw robust conclusions, it is imperative to analyze the fluctuations in mass density under varying plasma-β conditions. The influence of plasma β on mass density is clearly demonstrated in three temporal snapshots presented in Figures 5 through 8. This relationship is further highlighted in Figure 10, which illustrates density variations along the diagonal line y = x, underscoring the critical role of plasma β in modulating density profiles.

As noted earlier, the geometry of the magnetoacoustic pulse evolves from a circular to an elliptical configuration over time. The figures reveal that this transformation occurs more rapidly as the layer approaches the magnetic null point. For example, at the time instance t = 0.4 s, as shown in Figures 1 through 4, the pulse maintains its original shape at the radial layer r = 1, whereas it undergoes noticeable deformation at layers r = $\frac{1}{\sqrt{10}} \approx 0.32$ and r = $\frac{1}{10} = 0.1$. The proximity of the layer to the null point amplifies the extent of these morphological changes.

The findings reveal that the fast magnetoacoustic wave undergoes a refractive process, guiding it toward the magnetic null point, where it envelops the region. As the wave nears the null point, its velocity decreases, resulting in a contraction of spatial scales and a subsequent enhancement of current density in the surrounding area. In plasmas with β values approaching zero, the fast wave encounters an exponential surge in current density, as it is unable to propagate through the null point. This condition promotes highly effective dissipation of the linear fast magnetosonic wave, establishing null points as prime locations for plasma heating. In contrast, in environments with non-zero β, the presence of a finite sound speed allows the fast magnetosonic wave to traverse the null point, facilitating energy dissipation away from it. The dynamics of these interactions are governed by the plasma β parameter, which dictates the predominant physical effects observed. (see also [5]).

In accordance with the panels (a) of Figure 9, the red and orange lines ($\beta_0 = 0$ and 1, r = 1) exhibit significant spikes, indicating high values of radial velocity at specific points. The green line ($\beta_0 = 1$, r = 0.1) appears relatively flat, suggesting lower values of radial velocity. The panels (b) of Figures 9 show even more pronounced peaks, particularly around the null point. The orange line ($\beta_0 = 0$, r = 1) exhibits the highest peaks, indicating a strong response at those points. The other lines ($\beta_0 = 1$, r = 1, 0.32, 0.1) also display varying responses, but none reach the heights of the orange line. In accordance with the panels (c), the peaks remain present but appear more subdued compared to the panels (b). The orange line ($\beta_0 = 0$, r = 1) continues to be prominent, while the other lines demonstrate a more gradual increase and decrease in values. The overall trend suggests a stabilization of radial velocity values as we move away from the null point. In general, the plots demonstrate how radial velocity changes concerning the distance from the null point under varying conditions. The presence of sharp peaks signifies sensitivity to alterations in the parameters represented by the different lines. The overall trend across the plots indicates that as the x-values increase, the behavior of radial velocity stabilizes, especially under specific conditions. These visualizations may be valuable for examining the effects of various parameters on variable radial velocity in a particular context, potentially within a scientific or engineering application.

In accordance with the panels (a) of Figures 9, the red and orange lines ($\beta_0 \approx 0$ and 1, r = 1) show sharp peaks at the origin and around specific intervals, indicating high density values. The blue dotted line and green dashed line ($\beta_0 = 1$, r = 0.32, 0.1) exhibit lower density values, with the blue line displaying slight fluctuations. The overall trend indicates oscillations, with peaks occurring at regular intervals along the line y=x, particularly around the interval (0 – 3). The panels (b) of Figure 9 illustrate that the peaks for the red and orange

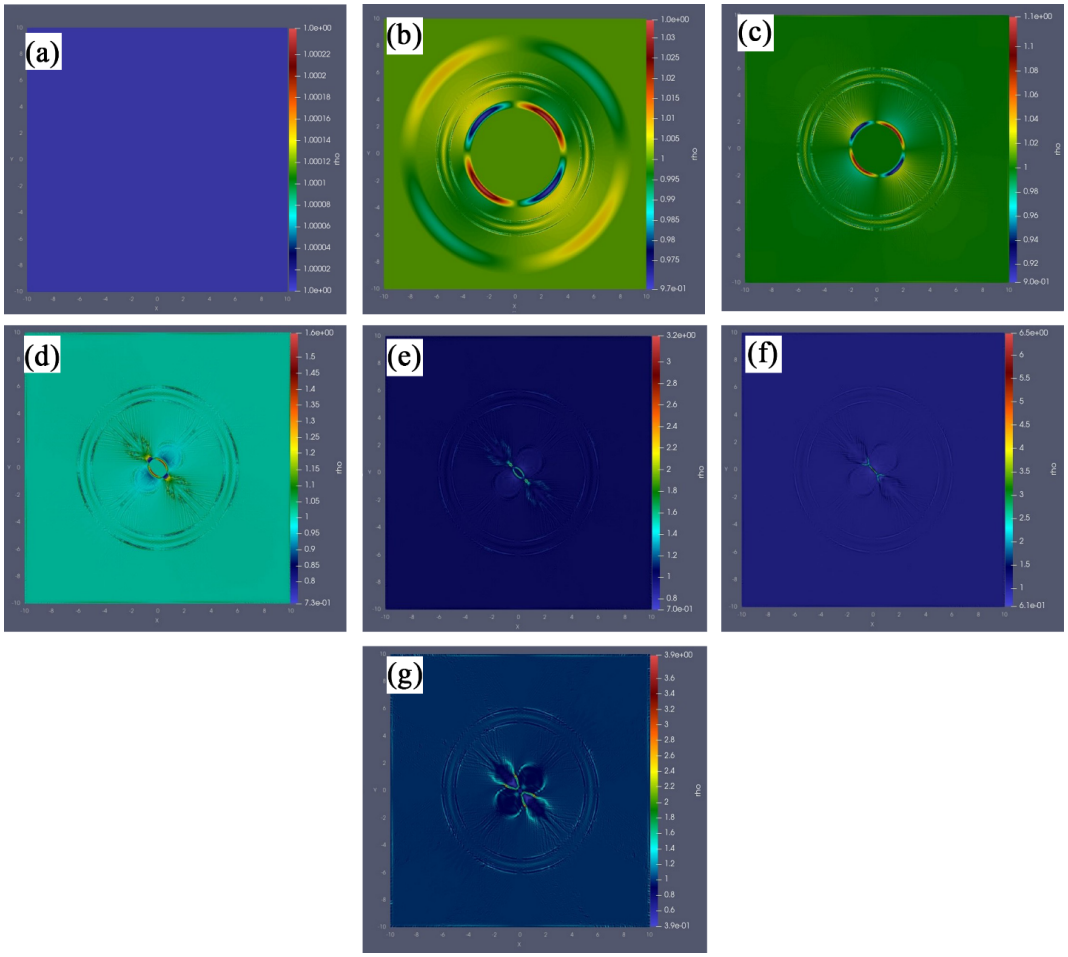

Figure 5: Temporal profiles of the plasma density for the inward-propagating rarefaction pulse are presented as functions of the radial coordinate r, with a plasma β value of $\beta_0 = 0$, evaluated at radial positions $r = 1$, $r = \frac{1}{\sqrt{10}}$, and $r = \frac{1}{10}$. These profiles are captured at the following time points: a) $t = 0$ s, b) $t = 0.4$ s, c) $t = 1$ s, d) $t = 2$ s, e) $t = 2.5$ s, f) $t = 3$ s, and g) $t = 4$ s.

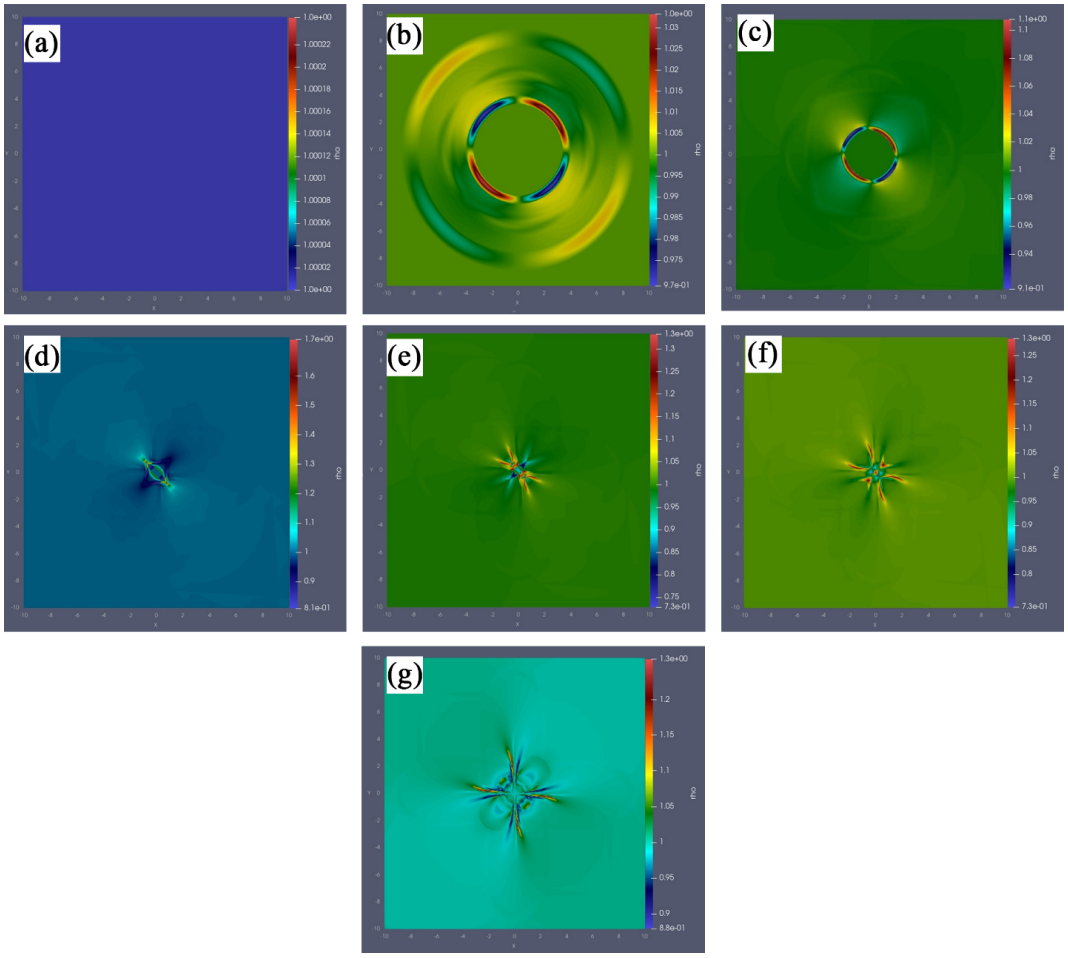

Figure 6: Temporal snapshots of the plasma density for the inward-propagating rarefaction pulse are presented as functions of the radial coordinate r, with a plasma β value of $\beta_0 = 1$, evaluated at the radial position $r = 1$. These profiles are captured at the following time instances: a) $t = 0$ s, b) $t = 0.4$ s, c) $t = 1$ s, d) $t = 2$ s, e) $t = 2.5$ s, f) $t = 3$ s, and g) $t = 4$ s.

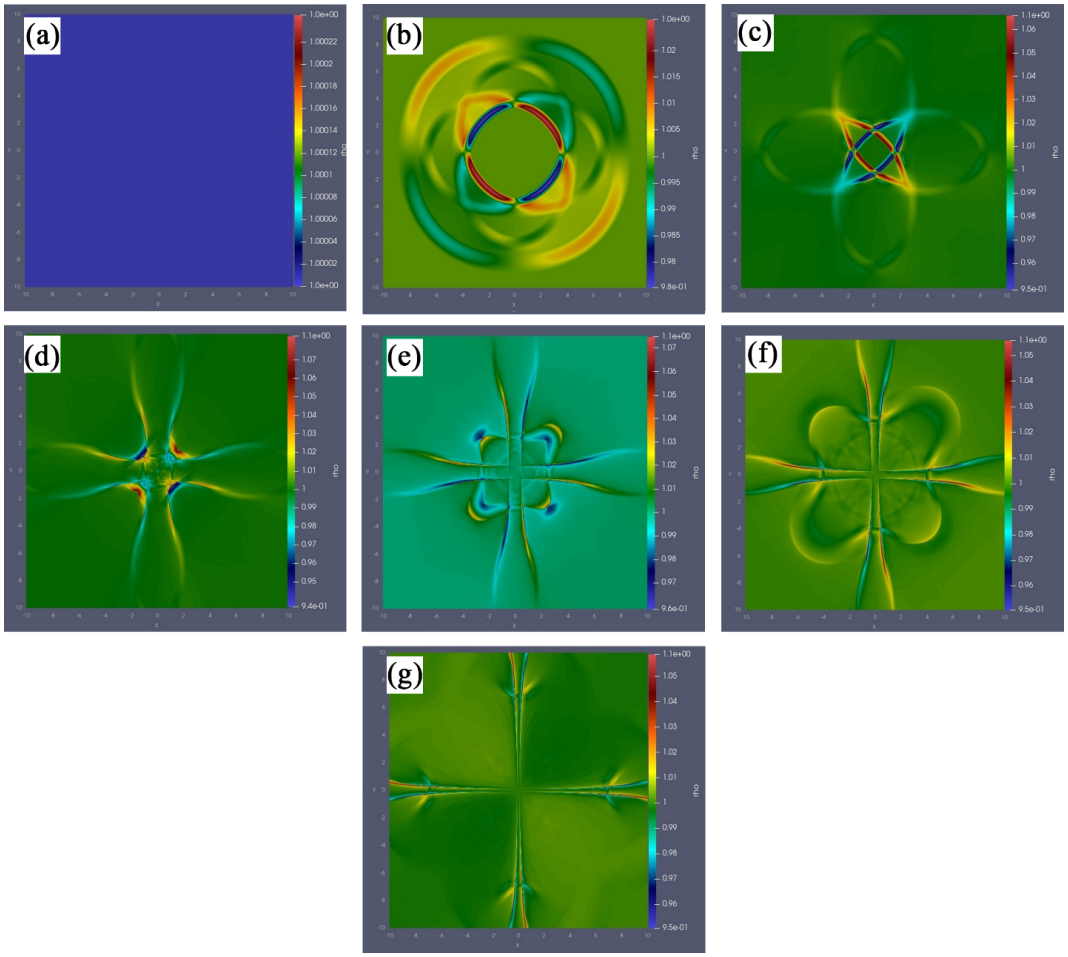

Figure 7: Temporal profiles of the plasma density associated with the inward-propagating rarefaction pulse are presented as functions of the radial coordinate r, with a plasma β value of $\beta_0 = 1$, evaluated at the radial position $r = \frac{1}{\sqrt{10}}$. These profiles are documented at the following time points: a) $t = 0$ s, b) $t = 0.4$ s, c) $t = 1$ s, d) $t = 2$ s, e) $t = 2.5$ s, f) $t = 3$ s, and g) $t = 4$ s.

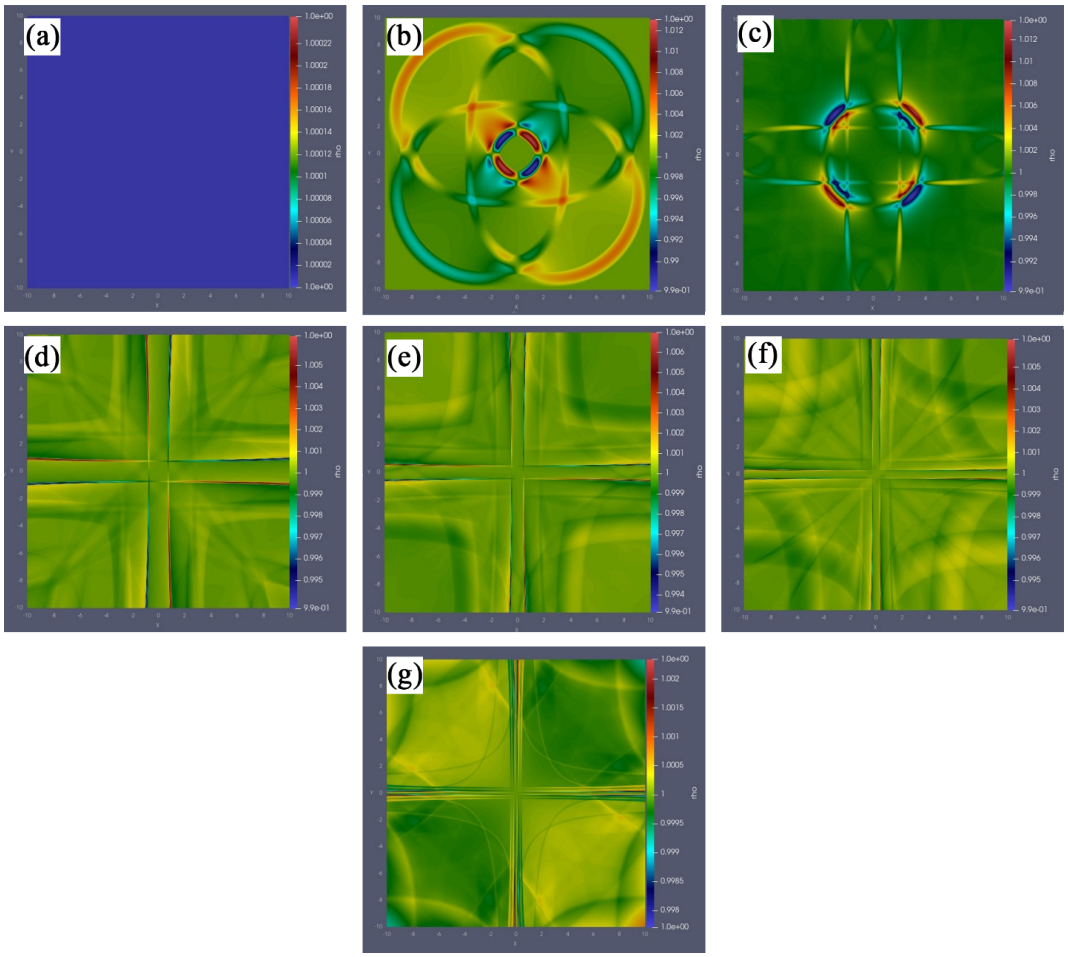

Figure 8: Temporal representations of the plasma density associated with the inward-propagating rarefaction pulse are illustrated as functions of the radial coordinate r, under conditions where the plasma β parameter is $\beta_0 = 1$, at the radial position $r = 0.1$. These density profiles are recorded at the following time points: a) $t = 0$ s, b) $t = 0.4$ s, c) $t = 1$ s, d) $t = 2$ s, e) $t = 2.5$ s, f) $t = 3$ s, and g) $t = 4$ s.

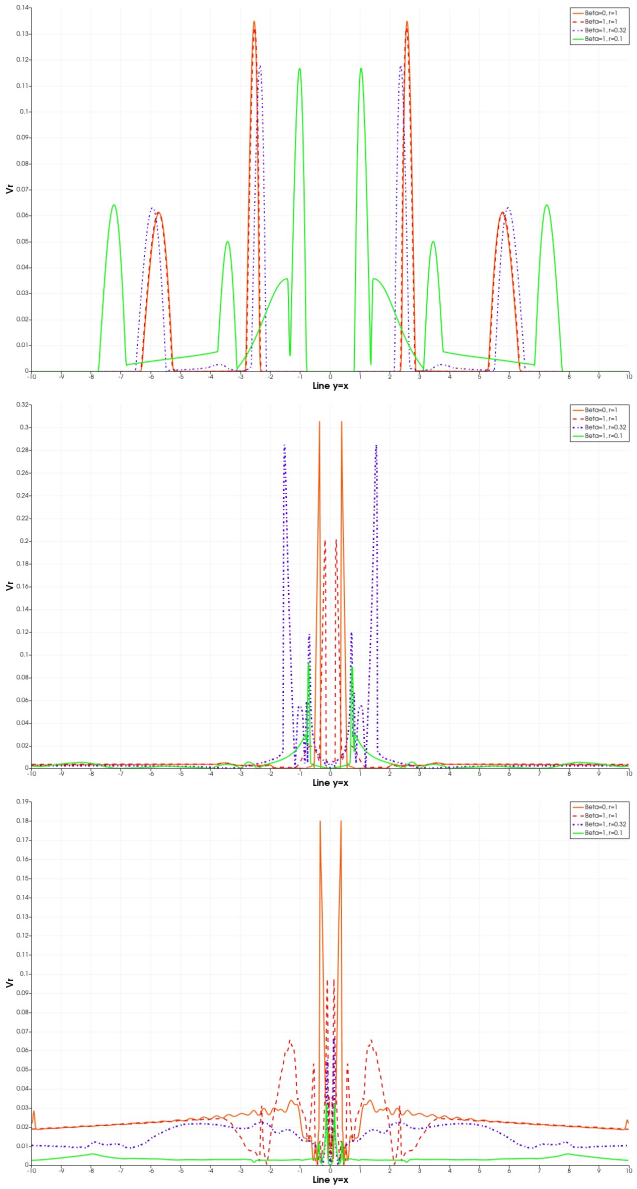

Figure 9: The analysis compares the radial velocity of the inward-propagating rarefaction pulse, defined as $v_r = \sqrt{v_x^2 + v_y^2}$, along the diagonal line $y = x$, under varying plasma β conditions and radial positions. Specifically, the comparison includes cases with $\beta_0 = 0$ at $r = 1$, $\beta_0 = 1$ at $r = 1$, $\beta_0 = 1$ at $r = \frac{1}{\sqrt{10}} \approx 0.32$, and $\beta_0 = 1$ at $r = \frac{1}{10} = 0.1$. These are evaluated at the following time instances: a) $t = 0.4$ s, b) $t = 2$ s, and c) $t = 4$ s.

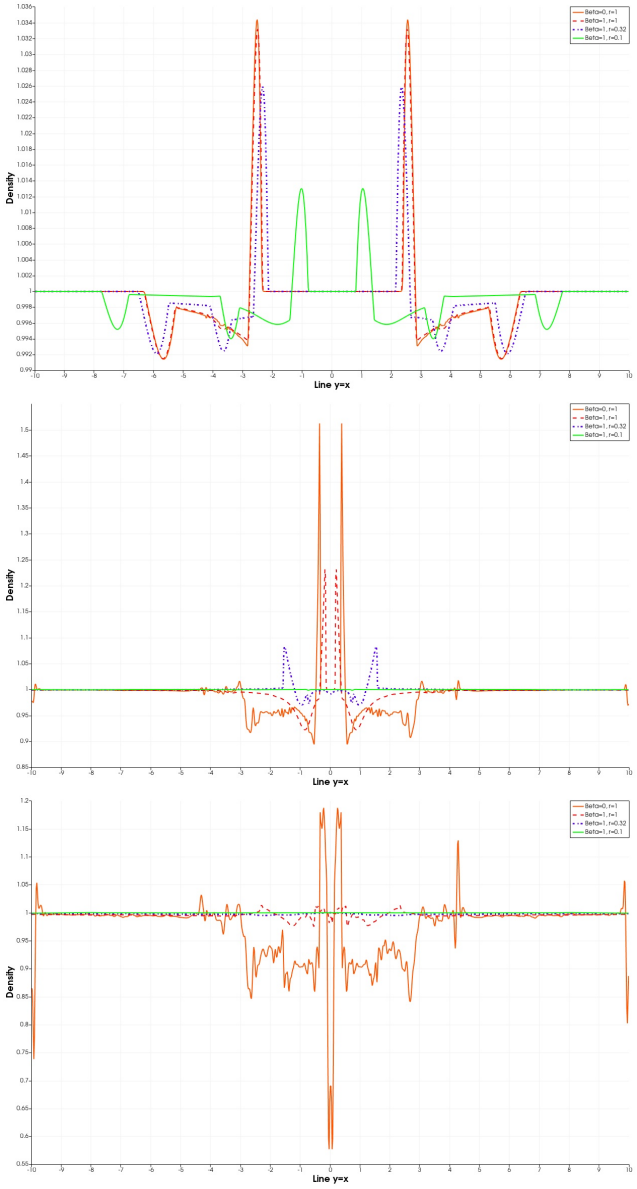

Figure 10: The analysis evaluates the plasma density variations along the diagonal line $y = x$ for different plasma β conditions and radial positions. Specifically, the comparison encompasses cases with $\beta_0 \approx 0$ at $r = 1$, $\beta_0 = 1$ at r =1, $\beta_0 = 1$ at $r = \frac{1}{\sqrt{10}} \approx 0.32$, and $\beta_0 = 1$ at $r = \frac{1}{10} = 0.1$. These density profiles are examined at the following time points: a) $t = 0.4$ s, b) $t = 2$ s, and c) $t = 4$ s.

lines ($\beta_0 = 0$ and 1, r = 1) are more pronounced compared to the panels (a), indicating a stronger density response at the near null point. The blue dotted line and green dashed lines ($\beta_0 = 1$, r = 0.32, 0.1) remain relatively stable, exhibiting only minor fluctuations. The overall shape suggests a concentrated response around the null point, highlighting a strong relationship between density and distance from the null point. In accordance with panels (c), the red and orange lines ($\beta_0 \approx 0$ and 1, r = 1) maintain their sharp peaks; however, the overall amplitude appears reduced compared to the second figure. The blue dotted line and green dashed line ($\beta_0 = 1$, r = 0.32, 0.1) exhibit more stable behavior, with less variation. The curves suggest a gradual leveling off, indicating that the density stabilizes as we move away from the null point.

5 Conclusions

This study has explored the complex dynamics of nonlinear magnetoacoustic wave pulses interacting with a two-dimensional magnetic null point, with particular emphasis on the spatial variability of the plasma beta parameter. Using high-resolution numerical simulations facilitated by the PLUTO code, we have demonstrated how fluctuations in plasma β, due to variations in magnetic field strength, critically influence wave behavior and plasma response in stratified atmospheric layers. Our results reveal that magnetoacoustic pulses exhibit significant deformation as they approach the null point, transforming from circular to elliptical wavefronts more rapidly in regions with higher plasma β values closer to the null point. The interaction leads to pronounced temporal changes in radial velocity and plasma density, marked by periodic amplitude fluctuations and sharp peaks, indicating episodes of enhanced energy coupling between the waves and the magnetic topology. Moreover, the findings underscore that in low-β environments, the fast magnetoacoustic wave is effectively trapped and dissipated near the null point, supporting the role of null points as key sites for plasma heating. Conversely, in environments with finite β, the wave can traverse the null region, with energy dissipation occurring over a broader spatial area. This highlights the crucial role of plasma β in governing wave propagation and dissipation mechanisms in solar coronal contexts, providing deeper insight into the underlying processes behind coronal heating. Overall, this work contributes to advancing our understanding of magnetohydrodynamic wave interactions in complex magnetic topologies and lays the groundwork for future studies addressing the nonlinear coupling between waves and magnetic reconnection in the solar atmosphere.

Acknowledgements

We gratefully acknowledge the support provided by Farhangian University for this research endeavor.

Authors' Contributions

The authors contributed to data analysis, drafting, and revising of the paper and agreed to be responsible for all aspects of this work.

Data Availability

Data will be made available on request. Correspondence and requests for data should be addressed to N. Karimi.

Conflicts of Interest

The author declares that there is no conflict of interest.

Ethical Considerations

The author has diligently addressed ethical concerns, such as informed consent, plagiarism, data fabrication, misconduct, falsification, double publication, redundancy, submission, and other related matters.

Funding

This research did not receive any grant from funding agencies in the public, commercial, or non profit sectors.

References

[1] Arregui, I., 2015, Philos. Trans. A Math. Phys. Eng. Sci., 373, 2.

[2] Petschek, H. E., 1964, NASA Spec. Publ., p. 425.

[3] Forbes, T. G., & Priest, E. R., 1987, Rev. Geophys., 25, 1583.

[4] Craig, I. J. D., & McClymont, A. N., 1991, Astrophys. J., 371, L41.

[5] McLaughlin, J. A., et al., 2009, A&A, 493, 227.

[6] Lee, E., Lukin, V. S., & Linton, M. G., 2014, A&A, 569, A94.

[7] Karimi, N., Alizadeh, M., & Shajei, Z., 2024, Iran. J. Astron. Astrophys., 11, 213.

[8] McLaughlin, J. A., Hood, A. W., & de Moortel, I., 2011, Space Sci. Rev., 158, 205.

[9] Kumar, P., et al., 2024, Nat. Commun., 15, 1.

[10] Priest, E., & Forbes, T., 2000, Magnetic Reconnection: MHD Theory and Applications, p. 612.

[11] Sabri, S., Ebadi, H., & Poedts, S., 2020, Astrophys. J., 902, 11.

[12] Goedbloed, J. P. H., & Poedts, S., 2004, Principles of Magnetohydrodynamics: With Applications to Laboratory and Astrophysical Plasmas, Cambridge Univ. Press, p. i.

[13] Nakariakov, V., & Kolotkov, D., 2020, Annu. Rev. Astron. Astrophys., 58, 1.

[14] Mignone, A., et al., 2007, Astrophys. J. Suppl. Ser., 170, 228.

[15] Mignone, A., et al., 2011, Astrophys. J. Suppl. Ser., 198, 7.

[16] Karampelas, K., et al., 2023, Astrophys. J., 943, 131.

[17] Gruszecki, M., et al., 2011, A&A, 531, A63.

[18] Galsgaard, K., Priest, E., & Titov, V., 2003, J. Geophys. Res. Space Phys., 108, A1.

[19] Thurgood, J., & McLaughlin, J., 2013, A&A, 555, A86.

[20] McLaughlin, J. A., Hood, A. W., & de Moortel, I., 2011, Space Sci. Rev., 158, 205.